

An almost-linear time decoding algorithm for quantum LDPC codes under circuit-level noise

Antonio deMarti iOlius,^{1,*} Imanol Etxezarreta Martinez,^{2,†} Joschka Roffe,^{3,‡} and Josu Etxezarreta Martinez^{1,§}

¹*Department of Basic Sciences, Tecnun - University of Navarra, 20018 San Sebastian, Spain.*

²*Independent researcher, San Sebastian, Spain.*

³*Quantum Software Lab, University of Edinburgh, United Kingdom.*

Fault-tolerant quantum computers must be designed in conjunction with classical co-processors that decode quantum error correction measurement information in real-time. In this work, we introduce the belief propagation plus ordered Tanner forest (BP+OTF) algorithm as an almost-linear time decoder for quantum low-density parity-check codes. The OTF post-processing stage removes qubits from the decoding graph until it has a tree-like structure. Provided that the resultant loop-free OTF graph supports a subset of qubits that can generate the syndrome, BP decoding is then guaranteed to converge. To enhance performance under circuit-level noise, we introduce a technique for sparsifying detector error models. This method uses a transfer matrix to map soft information from the full detector graph to the sparsified graph, preserving critical error propagation information from the syndrome extraction circuit. Our BP+OTF implementation first applies standard BP to the full detector graph, followed by BP+OTF post-processing on the sparsified graph. Numerical simulations show that the BP+OTF decoder achieves logical error suppression within an order of magnitude of state-of-the-art inversion-based decoders while maintaining almost-linear runtime complexity across all stages.

I. INTRODUCTION

Quantum error correction (QEC) is the key to operationally useful quantum computing and will enable the construction of fault-tolerant systems with capabilities well in excess of classical computing technologies [1]. The past decade has seen significant progress in experimental realisations of QEC, recently highlighted by the first demonstration by Google Quantum AI of a surface code logical qubit operating below the break-even point [2]. However, significant barriers remain to the practical realisation of QEC at scale. A particularly pertinent challenge relates to the problem of real-time decoding: the operation of a QEC code relies upon the ability to process vast quantities of syndrome information at timescales as low as $1\mu s$ [3] using classical co-processors [4]. As such, fast and accurate decoding algorithms are a critical component of the quantum computing stack.

Surface code QEC architectures are conceptually simple and can be implemented using local interactions between qubits arranged in a grid. However, a disadvantage of surface codes is that they have poor encoding rate and will require large qubit counts to achieve logical error rates in the *teraquop* regime (logical failure rate $p_F < 10^{-12}$) that is thought to be necessary to run algorithms that offer quantum advantage. Quantum low-density parity-check (QLDPC) codes are an alternative QEC protocol to the surface code and are suitable for quantum computing technologies that have high qubit

connectivity. Numerical simulations of QLDPC code architectures suggest that they will require approximately $10\times$ fewer qubits compared to surface code architectures [5–7]. However, the design of efficient decoding algorithms for QLDPC codes remains an open problem and a bottleneck to their implementation in experiment.

The belief propagation (BP) decoder is ubiquitous in classical communications, enabling real-time decoding for LDPC protocols underpinning technologies such as 5G, WiFi, and Ethernet [8]. The primary advantage of BP decoders lies in their speed: they can be executed on distributed hardware and have a linear worst-case runtime complexity of $\mathcal{O}(n)$ with respect to the code block length n [9]. However, when applied to QLDPC codes, BP decoders face significant challenges. These challenges stem from the presence of degenerate quantum errors and the emergence of trapping sets, which can prevent the BP decoder from converging [10, 11]. To address these issues, decoders for QLDPC codes typically augment BP with post-processing routines that are invoked when the main algorithm fails [12–18]. The most accurate of these two-stage algorithms — ordered statistics decoding (BP+OSD) [13, 14], ambiguity clustering (BP+AC) [16], and localized statistics decoding (BP+LSD) [18] — employ matrix inversion techniques to solve the decoding problem during post-processing. While these inversion-based decoders achieve high error thresholds, they also increase the worst-case runtime complexity to $\mathcal{O}(n^3)$. This is significantly slower than the $\mathcal{O}(n)$ runtime of standard BP. On the other hand, the closed-branch decoder (BP+CB) significantly reduces the worst-case runtime complexity, but is not as accurate as inversion-based decoders [17].

In this work, we present the ordered Tanner forest (OTF) algorithm as a post-processor to belief propagation that does not require matrix inversion. The core

* toni.demarti@gmail.com

† ietxezarretam@gmail.com

‡ joschka@roffe.eu

§ jetxezarreta@unav.es

idea behind OTF post-processing is based on the fact that the BP algorithm is guaranteed to converge when applied to decoding graphs with a tree-like structure. The OTF post-processor leverages this by constructing an ordered spanning tree of the QEC code's decoding (Tanner) graph, giving priority to nodes that were assigned a high probability of supporting an error during the initial BP decoding attempt. This spanning tree can contain multiple disconnected components, so we refer to it as an *ordered Tanner forest*. Once the ordered Tanner forest is formed, the BP algorithm can be applied directly to it to identify a decoding solution that aligns with the measured syndrome.

The OTF post-processor employs a modified version of Kruskal's algorithm to find the ordered Tanner forest, with a worst-case runtime complexity of $\mathcal{O}(n \log(n))$ [19]. This process involves searching through the nodes of the decoding graph and eliminating those that would introduce loops. A second round of BP is then run on the ordered Tanner forest, with a linear time complexity proportional to the number of remaining nodes. As a result, the combined BP+OTF decoder achieves an almost-linear runtime relative to the code's block length.

In practice, QEC decoding algorithms are run on a *detector* graph or detector error model which relates error mechanism in the QEC circuit to the measured syndromes [20]. A problem with applying OTF post-processing directly to the detector graph is that the columns are typically high-weight compared to the *code capacity* or *phenomenological* graph for the same code. As a consequence, it is often the case that many graph nodes need to be discarded in the search for the ordered Tanner forest, sometimes to the point where the remaining graph no-longer contains enough qubits to support a solution to the syndrome. To address this problem, we propose a novel procedure for mapping a detector graph to a *sparsified* detector graph with fewer short-length loops. When applied to this sparsified detector graph, OTF post-processing is more likely to succeed.

We propose a three-stage decoder specifically optimized for circuit-level noise which we refer to as BP+BP+OTF. First, standard BP decoding is applied to the full detector graph. Second, the soft-information output of the first BP round is mapped to the sparsified detector graph via a pre-defined transfer matrix. Using this soft-information as prior-information, BP decoding is applied a second time to the sparsified detector graph. Third, OTF post-processing is run on the sparsified detector graph guided by the soft-information output of the previous round of BP. Note that the BP+BP+OTF decoder terminates at the first successful decoding. E.g., the final round of OTF will not be invoked if either of the preceding rounds of BP succeeds.

To benchmark the BP+BP+OTF decoder, we run Monte Carlo simulations under depolarizing circuit-level noise for bivariate bicycle codes, specifically the $[[72,12,6]]$, $[[108,8,9]]$, and $[[144,12,12]]$ instances first investigated in [5]. Our results demonstrate that the

BP+BP+OTF decoder achieves error suppression performance that is within an order-of-magnitude of state-of-the-art BP+OSD decoders.

Our sparsification routine for detector error models is general, and has the potential to be useful for other families of decoders beyond BP+BP+OTF. For example, we observe that BP+BP+OSD decoders require considerably fewer BP iterations than is necessary for standalone BP+OSD applied to the full detector graph.

One of the key advantages of BP+BP+OTF is its simplicity: the decoder requires just three applications of a standard BP decoder and a single application of a modification of the well-known Kruskal algorithm for generating the ordered spanning forest. This straightforward design allows for the construction of highly efficient hardware implementations using off-the-shelf application-specific integrated circuits (ASICs). As a result, the BP+OTF decoder is an appealing option for decoding in near-term experiments.

II. PRELIMINARIES

A. Calderbank-Shor-Steane codes

Calderbank-Shor-Steane (CSS) codes describe a large family of quantum error correction protocols that can be expressed in terms of a pair of classical binary codes, $\mathcal{Q}(\mathcal{H}_X, \mathcal{H}_Z)$. The H_X matrix describes X -type stabilisers that detect phase-flip errors and the H_Z matrix Z -type stabilisers that detect bit-flip errors. If $H_{X/Z}$ are sparse, we can consider the CSS code to be a quantum LDPC code.

The decoding task for CSS codes involves solving two syndrome equations for X/Z errors

$$H_{X/Z} \cdot \mathbf{e}_{Z/X} \pmod{2} = \mathbf{s}_{X/Z}. \quad (1)$$

As the above syndrome equations amount to a pair of classical decoding problems, it is possible to use existing classical decoders to directly decode CSS codes. Note that the above syndrome equation is over binary field modulo-2. From this point onwards, we will assume all linear algebra operations are performed modulo-2 unless stated otherwise.

B. Belief propagation decoding

Belief propagation (BP) is common decoding algorithm in classical communication technologies [8, 9]. Decoders based on BP exploit the sparsity of the LDPC code's parity check matrix to efficiently solve the bit-wise decoding problem

$$p(\mathbf{e}_i) = \sum_{\sim_i} p(\mathbf{e}|\mathbf{s}). \quad (2)$$

The specific advantage of the BP decoder lies in its speed. The message passing operations that underpin the algorithm occur locally between the nodes of a graphical representation of the parity check matrix known as a Tanner graph, and can be run in parallel on distributed hardware. In this setting, BP has a worst-case runtime complexity $\mathcal{O}(n)$ in the code's block-length n .

The product-sum algorithm is a variant of the BP decoder that is known to yield exact marginals for parity check matrices that have tree-like Tanner graphs. In practice, however, most high-rate LDPC codes contain loops that compromise the performance of product-sum BP and can prevent it from converging to a valid solution. A challenge in designing LDPC codes lies in finding parity check matrices that are sufficiently loop-free and sparse.

For quantum LDPC codes, it is particularly difficult to design H_X and H_Z matrices that are well-suited for BP decoding. The reason for this can be attributed to degenerate errors that lead to cyclic dependencies in the decoding graph. As such, BP-based algorithms typically do not work as effective decoders for quantum LDPC codes. Indeed, a standard implementation of product-sum BP fails to yield a threshold for the surface code [14]. In practice, quantum decoders require BP to be augmented with a post-processing routine to achieve satisfactory performance in terms of both threshold and sub-threshold error suppression [12–18].

C. Decoding circuit-level noise and the detector error model

In classical error correction, the decoding problem involves directly solving the syndrome equation $H \cdot \mathbf{e} = \mathbf{s}$, where H is the parity-check matrix of the code. In quantum error correction, however, an additional layer of complexity arises due to the fact that syndromes are measured using noisy circuits, leading to error propagation that is not described by the CSS code's $H_{X/Z}$ matrices. Instead, the circuit-level decoding problem is characterised by a binary matrix, H_{CL} , where the columns correspond to error mechanisms within the circuit, and the rows correspond to syndrome measurements. For instance, a non-zero entry at position $(H_{CL})_{ij}$ indicates that error mechanism j triggers syndrome measurement i . Once the circuit-level matrix H_{CL} is constructed, the decoding problem becomes equivalent to that of decoding a classical linear code, specifically solving $H_{CL} \cdot \mathbf{e} = \mathbf{s}$. The key conceptual difference is that the columns of H_{CL} represent circuit error mechanisms, rather than Pauli- X/Z errors, as is the case in code capacity decoding using the $H_{X/Z}$ CSS matrices.

In practice, QEC protocols operate by repeatedly measuring the same stabiliser extraction circuit over time. This repeating structure can be leveraged to simplify the circuit-level decoding problem by mapping it to a *detector error model* [20]. A detector vector is defined as a lin-

ear combination of syndrome measurements that sums to zero when there are no errors in the circuit. In a repeated stabiliser measurement circuit, the most intuitive choice of detectors involves comparing the parity between consecutive syndrome measurements. For example, if the same check yields a value of 1 in two consecutive rounds, the detector value will be trivial. The resulting detector vector \mathbf{s}_D is therefore sparser than the original syndrome \mathbf{s} . Correspondingly, the circuit-level decoding matrix H_{CL} is replaced with a detector matrix H_{dem} , as a $d \times n$ binary matrix, where d is the number of measurements (detector elements) and n is the number of possible errors in the circuit [21]. Here, the rows correspond to detector measurements rather than syndromes. Typically, H_{dem} is also sparser than H_{CL} . This sparser structure of the detector error model, described by the equation $H_{dem} \cdot \mathbf{e} = \mathbf{s}_D$, makes the decoding problem more amenable to BP decoding. From this point onwards, we will refer to \mathbf{s} as a syndrome (code capacity, phenomenological noise) or a detector (circuit-level noise) interchangeably.

Once a set of fault-mechanisms $\hat{\mathbf{e}}$ have been identified by decoding the detector error model $H_{dem} \cdot \mathbf{e} = \mathbf{s}$, the task remains to determine their logical action. This can be analysed using the logical observable matrix, $O_{dem} \in \mathbb{F}^{k \times n}$, where k is the number of logical qubits encoded, and n represents the number of possible fault mechanisms in the detector error model. This matrix links errors in the circuit to measured logical observables, which are defined as binary sums of measurements that correspond to the outcomes of logical operator measurements for any logical state encoded by the QEC code. The logical observable matrix associated with the detector error model is crucial for verifying whether the error estimate produced by the decoder successfully corrects the actual faults that occurred. A logical error is detected if the logical observable derived from the decoded error does not match the true logical observable, i.e., if $O_{dem} \cdot \mathbf{e} \neq O_{dem} \cdot \hat{\mathbf{e}}$.

The detector error model, as well as the the logical observable matrix for a specific detector error model related to the syndrome extraction circuit can be generated using a stabiliser simulator [22, 23].

III. THE ORDERED TANNER FOREST DECODER, AN ALMOST-LINEAR TIME POST-PROCESSOR

In this section, we introduce the ordered Tanner forest (OTF) decoder as an almost-linear post-processor for general QLDPC codes. The OTF decoder is a post-processing algorithm that is invoked if the original round of BP decoding fails, i.e., when the estimated BP error $\hat{\mathbf{e}}_{BP}$ does not satisfy the syndrome equation, $H \cdot \hat{\mathbf{e}}_{BP} \neq \mathbf{s}$. Being a post-processor, OTF requires the posterior probabilities coming from a BP decoding stage (or some process able to provide soft reliability information) and is

only invoked when BP does not converge. Based on the received soft information, we sort the columns of the parity check matrix from the least reliable to the most reliable [4]. The OTF post-processor then works by deleting columns in the ordered parity check matrix to obtain a reduced parity check matrix, H_{otf} , that maps to a Tanner graph that is completely loop free. Note that the resultant spanning tree may contain multiple disconnected trees, so we refer to the returned structure as an *ordered Tanner forest* (OTF). A product-sum BP decoder is then applied to solve the reduced decoding problem $H_{otf} \cdot \mathbf{e}_{otf} = \mathbf{s}$. As the H_{otf} matrix has a tree-like structure, the second round of BP is guaranteed to converge if a solution exists, i.e., if \mathbf{s} is linearly dependent on the columns of H_{otf} such that $\mathbf{s} \in \text{IMAGE}(H_{otf})$.

A loop-free graph can be obtained from any parity check matrix through the application of Kruskal's minimum spanning tree algorithm [19]. This algorithm iterates through every node in the graph, eliminating those that introduce loops in the Tanner graph. An example of an OTF instance over a Tanner graph is shown in Figure 1. Note that a slight reinterpretation of the original Kruskal algorithm, as presented in [19], is necessary to adapt it to Tanner graphs. Specifically, while the original algorithm focuses on excluding certain graph edges, the modified version instead considers the data nodes of the Tanner graph. With this adjusted perspective, the modified algorithm can be implemented exactly as described in [19].

The BP+OTF decoding process can now be summarised as follows:

1. Attempt to solve to the decoding using BP on the full parity check matrix. If $H \cdot \hat{\mathbf{e}}_{BP} = \mathbf{s}$, return $\hat{\mathbf{e}}_{BP}$ as the solution. Else, proceed to step 2.
2. Use the soft-information output of the BP decoding, $p_{BP}(\mathbf{e})$, to order the qubits from most-to-least likely of being in the support of the error.
3. Apply the modified Kruskal algorithm to the parity check matrix, considering qubits in the order determined in step 2, to obtain the OTF parity check matrix H_{otf} .
4. Solve the OTF decoding problem using a product-sum BP decoder.
5. Verify the output of the OTF decoding: if $H_{otf} \cdot \hat{\mathbf{e}}_{otf} = \mathbf{s}$, then the decoding is valid. This will be the case for all instance of H_{otf} where $\mathbf{s} \in \text{IMAGE}(H_{otf})$, assuming that the BP decoder has been allowed to run for a number of iterations equal to the column count of H_{otf} .

A. Complexity of OTF post-processing

The runtime complexity of each of the steps in OTF post-processing is outlined below:

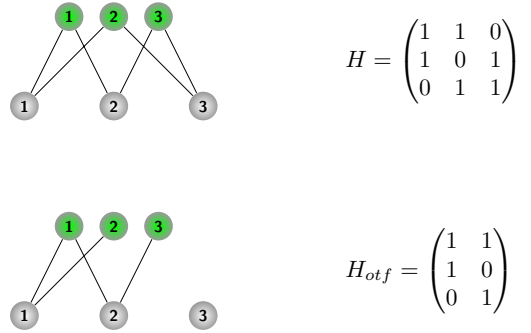


Figure 1: Top: the Tanner graph of a classical cyclic code altogether with its parity check matrix H . Grey circles denote bits and green circles parity checks. Bottom: the ordered Tanner forest generated by the OTF algorithm and its corresponding parity check matrix H_{otf} . Note that the third bit has been removed from the graph. This ensures that the H_{otf} matrix is cycle free.

1. Sorting qubits by probability of error: the columns of the parity check matrix are sorted in order of decreasing probability of being in error. Such a sort can be computed with complexity $\mathcal{O}(n \log(n))$, e.g. by means of a merge sort algorithm [24].
2. Computing the ordered Tanner graph H_{otf} . The OTF can be obtained with complexity $\mathcal{O}(n \log(n))$, using Kruskal's algorithm [19] (see Appendix A for more details).
3. Belief propagation over the OTF graph. This has worst-case runtime $\mathcal{O}(n)$, where n is the block-length of the code [9].

The complexity is dominated by the second step with runtime $\mathcal{O}(n \log n)$. Thus, the OTF decoder therefore has almost-linear time complexity with the block-length of the code.

B. Graph sparsity and OTF graph validity

The OTF post-processor can be viewed as an approximate matrix inversion method: by generating a spanning tree of the original graph, it seeks to identify a set of linearly independent columns that can reproduce the syndrome. This set of columns can be identified in $\mathcal{O}(n \log(n))$ time, which is a significant improvement over the $\mathcal{O}(n^3)$ worst-case complexity of matrix inversion via Gaussian elimination. However, unlike Gaussian elimination, Kruskal's algorithm does not guarantee that a compatible set of linearly independent columns will be found such that $\mathbf{s} \in \text{IMAGE}(H_{otf})$.

The success of OTF post-processing is closely tied to the sparsity of the parity-check matrix's columns: the lower the average column weight \bar{j} , the more likely it is to find a valid ordered Tanner forest H_{otf} . To understand this, consider the process by which the OTF matrix is constructed. The search begins with an empty matrix H_{otf}^0 . The OTF matrix is then populated by adding columns from the original matrix, H , that do not introduce loops into H_{otf}^i , where i denotes the tree growth step (i.e., the number of columns added so far). At each growth step i , the Tanner graph of H_{otf}^i is represented as $\mathcal{T}^i(V_D, V_P, E)$, where V_D are the data nodes, V_P are the parity nodes, and E are the edges. Each column under consideration from H can similarly be represented as a set of parity nodes \tilde{V}_P , with the column weight j defined as $|\tilde{V}_P|$.

For a new column to introduce a loop in H_{otf} , it must satisfy the condition $|\tilde{V}_P \cap V_P| > 1$. Therefore, a lower average column weight \bar{j} will lead to a higher chance that a new column will not produce a loop. Consequently, a sparser graph is more likely to result in an ordered Tanner forest H_{otf} with a greater number of linearly independent columns, thereby increasing the probability that the condition $\mathbf{s} \in \text{IMAGE}(H_{otf})$ is satisfied.

IV. SPARSIFYING DETECTOR ERROR MODELS

As described in Section II C, QEC codes are decoded by means of a detector graph that relates circuit fault locations to linear combinations of syndrome measurements. The detector error model enables the propagation of errors through the syndrome extraction circuit to be accounted for during decoding. Due to the richer set of error mechanisms it accounts for, it is typically the case that a detector error model graph will be less sparse than the corresponding CSS parity check matrices $H_{X/Z}$ of the code. This lack of sparsity is detrimental to the success of OTF post-processing, as it increases the probability that the generated OTF matrix will not satisfy the validity condition $\mathbf{s} \in \text{IMAGE}(H_{otf})$. See Section III B for more details.

We now describe a *sparsification* routine which is designed to re-express a detector error model graph into a sparser form that is more suitable for OTF decoding. Specifically, our method maps the detector graph $H_{dem} \in \mathbb{F}_2^{d \times n}$ into a sparsified detector graph $H_{sdem} \in \mathbb{F}_2^{d \times n_s}$ that has maximum column weight at most equal to the maximum column-weight, γ , of $H_{X/Z}$. This is achieved by finding linear-combinations of columns of weight $\leq \gamma$ that generate each of the columns in H_{dem} . As the H_{sdem} matrix is by design sparser and smaller than the detector matrix H_{dem} , applying OTF post-processor H_{sdem} is more likely to result in a successful decoding.

Our mapping includes a *transfer matrix* that allows the error channel associated with each error mechanism in the detector graph to be mapped to an equivalent er-

ror channel for the sparsified detector graph. This enables the soft-information output of an initial run of BP applied to the detector model to be re-purposed in the sparsified detector graph. The benefit of this is two-fold: first, the sparsified detector graph decoding will account for aspects of error propagation through the circuit, and second, the BP decoding over the OTF graph will be over a non-uniform noise channel, improving its rate of convergence.

The sparsification routine is motivated by techniques used to map detector error models for surface codes to graphs with column-weight ≤ 2 suitable for decoding with matching decoders such as minimum-weight perfect-matching [25] or union-find [26]. Furthermore, the transfer matrix is a generalization of the methods proposed for mapping circuit-level soft-information in [27].

We now formally define the sparsified detector error model and its corresponding transfer matrix.

Definition 1 (The sparsified detector matrix)

The detector error model is a $d \times n$ binary matrix $H_{dem} = (\mathbf{h}_{dem}^1, \mathbf{h}_{dem}^2, \dots, \mathbf{h}_{dem}^n)$, where $\mathbf{h}_{dem}^i \in \mathbb{F}_2^d$ is the binary vector representing the i^{th} column. Let Λ be a list of n_s indices denoting all columns in H_{dem} that have Hamming weight $|\mathbf{h}_{dem}^i| \leq \gamma$, where γ is the maximum Hamming weight of a column in the code's CSS matrices $H_{X/Z}$. The sparsified detector model, H_{sdem} , is a $d \times n_s$ sub-matrix of the detector model $H_{sdem} \subseteq H_{dem}$, formed by selecting the low-weight columns of H_{dem} indexed by Λ . Similarly, the sparsified logical observable matrix O_{sdem} is composed of the subset of columns of O_{dem} indexed by Λ .

Recall that each column in a detector error model matrix, H_{dem} , corresponds to a fault mechanism in the code's syndrome extraction circuit, each of which triggers a sequence of detectors indexed by the non-zero entries in the column. As such, H_{sdem} represents a reduced set of error mechanisms. We now define the transfer matrix that relates the full detector error model to its sparsified form:

Definition 2 (The transfer matrix) The transfer matrix $A_{tr} \in \mathbb{F}_2^{n_s \times n}$ describes the mapping from sparsified detector model to the full detector error model

$$H_{sdem} \cdot A_{tr} = H_{dem}. \quad (3)$$

Each column \mathbf{a}^i of A_{tr} is a vector that maps column \mathbf{h}_{dem}^i of H_{dem} to a linear combination of the columns of H_{sdem}

$$\mathbf{h}_{dem}^i = \sum_j a_j^i \mathbf{h}_{sdem}^j. \quad (4)$$

The transfer matrix preserves the action of the logical observable matrix such that

$$O_{dem} \cdot \mathbf{e}_{dem}^i = O_{sdem} \cdot \left(\sum_j a_j^i \mathbf{e}_{sdem}^j \right), \quad (5)$$

where \mathbf{e}_{dem}^i and \mathbf{e}_{sdem}^j refer to the circuit faults associated to columns i and j of the detector and sparsified models accordingly.

Importantly, the decomposition given by the transfer matrix maps the faults of the detector error model to combinations of faults on the sparser detector graph with *the same logical action*. Note, also, that the transfer matrix is not unique: multiple decompositions of the columns of H_{dem} into components of H_{sdem} are possible. Our primary objective is to identify sparse transfer matrices, where each column \mathbf{a}^i in A_{tr} has the smallest possible Hamming weight. This is crucial because the transfer matrix inherently maps low-weight fault mechanisms in the detector error graph to higher-weight errors in the sparsified graph. By ensuring the transfer matrix is sparse, we minimise the likelihood that the mapped errors will exceed the code distance. Additionally, a sparse transfer matrix is advantageous for mapping soft-information to the sparsified detector graph, as will be expanded upon in the next section.

The question as how to best optimise the transfer matrix is an interesting question for future work. For the QEC codes simulated in this work, we found that an exhaustive search method was sufficient. Details of our exhaustive strategy are outlined in Appendix B.

A. Belief propagation decoding using the sparsified detector graph

In this section, we propose a two stage BP+BP decoder, where BP is first applied to the full detector model graph followed by a second round of decoding on the sparsified detector graph. To this end, we outline a procedure that uses the transfer matrix to translate the soft-information output of the first round of BP into a form that can be used as the initial error channel for the second round of BP. This ensures that the decoding on the sparsified graph accounts for information about error propagation at the circuit-level. Furthermore, as the second round of BP will be supplied with a non-uniform error channel, it is more likely to converge to a solution satisfying the syndrome.

After completing the first round of BP on the full detector graph, we obtain the decoder's soft-information output, denoted as $p_{BP}(\mathbf{e}_{dem})$. This output assigns an error probability to each fault mechanism in the detector model H_{dem} . Our objective is to develop a method to translate $p_{BP}(\mathbf{e}_{dem})$ into a corresponding probability vector $p(\mathbf{e}_{sdem})$, which allocates error probabilities to each fault mechanism in the sparsified detector error model H_{sdem} .

The transfer matrix A_{tr} establishes a relationship between fault mechanisms in the detector model and those in the sparsified detector model. Specifically, the list of detector fault mechanisms that trigger a given fault mechanism i in the sparsified model is represented by $\{j : A_{tr}^{ij} \neq 0\}$.

When combining multiple error probabilities from the detector graph into a single probability for the sparsified graph, it is crucial to account for parity. For instance, if two individual error mechanisms in the detector error model, \mathbf{e}_{dem}^1 and \mathbf{e}_{dem}^2 , trigger the same component in the sparsified detector matrix, \mathbf{e}_{sdem}^k , their combined effect would be $(\mathbf{e}_{sdem}^k + \mathbf{e}_{sdem}^k) \bmod 2 = \mathbf{0}$. Therefore, probabilities should be summed only when an odd number of detector fault mechanisms contribute to the relevant sparsified detector fault mechanism. Thus, we want to determine the probability of the sparsified faults as the random variable defined as the modulo-2 sum (parity constraint) of the binary random variables associated to the detector error model faults that relate to it via A_{tr} . This mapping of probabilities from H_{dem} to H_{sdem} can then be accomplished by considering the probability of the exclusive OR (XOR) of the component binary random variables, as follows [28]

$$p(\mathbf{e}_{sdem}^i) = p \left(\bigoplus_{k \in \{j : A_{tr}^{ij} \neq 0\}} \mathbf{e}_{dem}^k \right) = \frac{1}{2} \left(1 - \prod_{k \in \{j : A_{tr}^{ij} \neq 0\}} (1 - 2p(\mathbf{e}_{dem}^k)) \right), \quad (6)$$

where by A_{tr}^{ij} we refer to element j of row i of the transfer matrix, \oplus refers to the XOR operation and by \mathbf{e}_{sdem}^i and \mathbf{e}_{dem}^k we refer to the binary random variables associated to the sparsified and circuit faults i and k , respectively. The combined probability in expression 6 can be derived by means of the Piling-up lemma that describes the probability of the XOR-clause of n independent binary random variables [29], which is the case discussed here.

Algorithm1 BP+BP decoder for circuit-level noise

INPUT: Measured syndrome $\mathbf{s} \in \mathbb{F}_2^d$
A priori probabilities of detector error model mechanisms, $p_{ch} \in \mathbb{R}^n$
Detector matrix: $H_{dem} \in \mathbb{F}_2^{d \times n}$,
Sparsified detector matrix: $H_{sdem} \in \mathbb{F}_2^{d \times n_s}$,
Transfer matrix: $A_{tr} \in \mathbb{F}_2^{n_s \times n}$
OUTPUT: Estimated error, $\hat{\mathbf{e}}$.

```

1:  $(\hat{\mathbf{e}}_{dem}, p(\mathbf{e}_{dem})) \leftarrow \text{BP\_decode}(\mathbf{s}, p_{ch}, H_{dem})$ 
2: if  $\mathbf{s} == \hat{\mathbf{s}}_{dem}$  then
3:   return  $\hat{\mathbf{e}}_{dem}$ 
4: end if
5:  $p(\mathbf{e}_{sdem}) \leftarrow \text{Map}(p(\mathbf{e}_{dem}), A_{tr})$ 
6:  $\hat{\mathbf{e}}_{sdem} \leftarrow \text{BP\_decode}(\mathbf{s}, p(\mathbf{e}_{sdem}), H_{sdem})$ 
7: return  $\hat{\mathbf{e}}_{sdem}$ 

```

The complete BP+BP algorithm is outlined in Algorithm 1. Both stages of the BP algorithm run in linear time. To fully understand the performance of the

BP+BP decoder, we need to analyse the runtime scaling of the mapping from the detector error model to the sparsified model. To this end, it is insightful to treat the transfer matrix A_{tr} as analogous to a Tanner graph, where the variable nodes represent elements of the detector error model, and the check nodes correspond to elements of the sparsified detector error model. Equation 6 can be interpreted as a message-passing update from the variable nodes to the check nodes. By using the soft information from the first BP update round as the a posteriori soft information, the probabilities $p(e_{s_{dem}}^i)$ can be computed in a single message-passing step. The computational complexity of this mapping process is essentially equivalent to that of running BP. The key difference is that the column weight is now determined by the transfer matrix, which is not uniquely defined. However, in all QEC codes examined in this study, the transfer matrices did not exhibit column weights exceeding 3, suggesting that it is generally lower than the column weight of the detector error model. Therefore, the worst-case complexity of the overall BP+BP decoder can be bounded by $\mathcal{O}(n)$, indicating linear time complexity.

V. AN ALMOST-LINEAR TIME DECODER FOR QLDPC CODES UNDER CIRCUIT-LEVEL NOISE

We now outline BP+BP+OTF as a decoding method with almost-linear runtime complexity for QLDPC codes operating under circuit-level noise. The decoder first runs the two-stage BP+BP decoder on the detector graph and its corresponding sparsified graph as described in the previous section. If BP+BP fails, the OTF decoder is applied to the sparsified graph as a post-processor. Pseudo-code for the BP+BP+OTF decoder is provided below:

Algorithm2 BP+BP+OTF decoder for circuit-level noise

INPUT: Measured syndrome: $\mathbf{s} \in \mathbb{F}_2^d$
a priori probabilities of DEM error mechanisms, $p_{ch} \in \mathbb{R}^n$
Detector matrix: $H_{dem} \in \mathbb{F}_2^{d \times n}$,
Sparsified detector matrix: $H_{s_{dem}} \in \mathbb{F}_2^{d \times n_s}$,
Transfer matrix: $A_{tr} \in \mathbb{F}_2^{n_s \times n}$
OUTPUT: Estimated error, $\hat{\mathbf{e}}$.

```

1:  $(\hat{\mathbf{e}}_{dem}, p(\mathbf{e}_{dem})) \leftarrow \text{BP\_decode}(\mathbf{s}, p_{ch}, H_{dem})$ 
2: if  $\mathbf{s} == \hat{\mathbf{s}}_{dem}$  then
3:   return  $\hat{\mathbf{e}}_{dem}$ 
4: end if
5:  $p(\mathbf{e}_{s_{dem}}) \leftarrow \text{Map}(p(\mathbf{e}_{dem}), A_{tr})$ 
6:  $(\hat{\mathbf{e}}_{s_{dem}}, p(\mathbf{e}_{s_{dem}})) \leftarrow \text{BP\_decode}(\mathbf{s}, p(\mathbf{e}_{s_{dem}}), H_{s_{dem}})$ 
7: if  $\mathbf{s} == \hat{\mathbf{s}}_{s_{dem}}$  then
8:   return  $\hat{\mathbf{e}}_{s_{dem}}$ 
9: end if
10:  $\hat{\mathbf{e}}_{otf} \leftarrow \text{OTF}(H_{s_{dem}}, p(\mathbf{e}_{s_{dem}}))$ 
11: return  $\hat{\mathbf{e}}_{otf}$ 

```

The runtime complexity of this decoder is dominated by the $\mathcal{O}(n \log(n))$ complexity of the OTF post-processing stage. As such, the full BP+BP+OTF decoder is an almost-linear time decoder for circuit-level decoding of QLDPC codes.

VI. RESULTS

We numerically benchmark the performance of the BP+BP+OTF decoder via Monte Carlo simulations of the bivariate bicycle codes under a depolarising circuit-level noise model [5]. Precise details of the numerical methods used for this section can be found in Appendix C, whilst a detailed specification of the circuit-level noise model is outlined in Appendix D.

To demonstrate the versatility of the sparsified detector model mapping, we conduct tests with various BP-based decoders. One key advantage of the detector error model sparsification technique is its ability to significantly reduce the total number of iterations required for BP to converge. Below, we outline the decoders we simulate, along with the specific BP iteration counts used for each:

- **Belief propagation (BP):** 1000 iterations over the detector error model graph.
- **Two-stage belief propagation (BP+BP):** 30 iterations over the detector error model and 100 iterations over the sparsified detector graph.
- **Two-stage BP + ordered Tanner forest (BP+BP+OTF):** 30 iterations over the detector error model, 100 iterations over sparsified detector graph and 100 for solving the Tanner forest.
- **Belief propagation + ordered statistics decoding (BP+OSD):** 1000 iterations over the detector error model Tanner graph.
- **Two-stage BP + OSD (BP+BP+OSD):** 30 iterations over the detector error model and 100 over the sparsified detector error model.

Note that the iteration numbers used for the different decoding algorithms vary significantly. The primary motivation for this variation is to demonstrate that, by employing the proposed detector error model sparsification technique, far fewer iterations of BP are necessary. This reduction in iterations leads to a substantial decrease in runtime over a straight-forward application of BP for N_{BP} iterations.

A. Bivariate bicycle codes

Figure 2 shows the results of Monte Carlo decoding simulations for families of bivariate bicycle codes. Decoding simulations were run for the $[[72, 12, 6]]$, $[[108, 8, 10]]$,

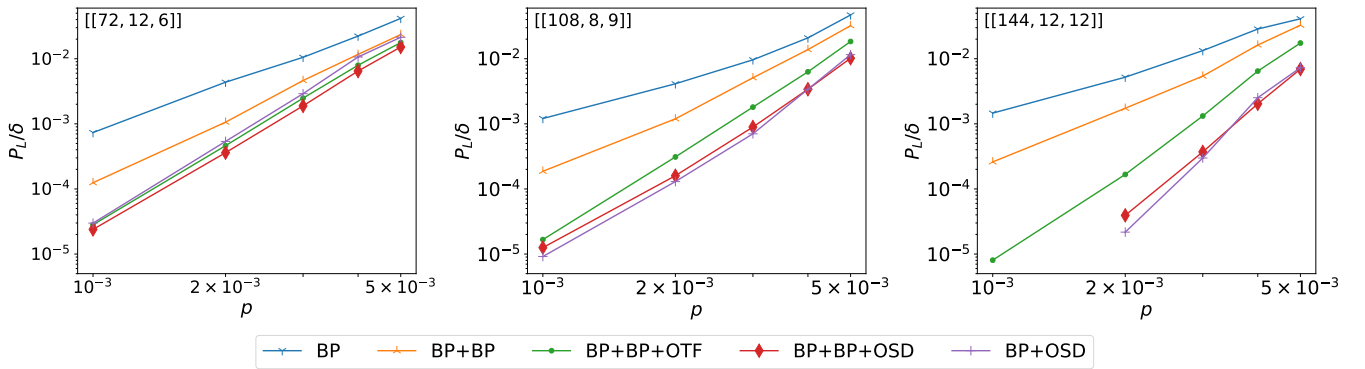


Figure 2: Logical error rate per syndrome extraction round with dependence on the physical error rate for three bivariate bicycle codes under different circuit-level decoding strategies. The left, middle and right plots correspond to bivariate bicycle codes with $l = 6, 9$ and 12 respectively, $m = 6$, $A = x^3 + y + y^2$ and $B = y^3 + x + x^2$. Each code is simulated over a number of syndrome rounds equal to its distance δ .

and $[[144, 12, 12]]$ bivariate bicycle codes first introduced in [5]. Notably, the proposed BP+BP protocol significantly enhances performance compared to running BP directly on the detector error model Tanner graph across all the codes. Specifically, we observe nearly an order-of-magnitude reduction in the logical error rate. Importantly, this improvement is achieved with approximately 90% fewer overall BP iterations (1000 vs. 130), resulting in a significantly reduced runtime. However, the results also indicate that simply increasing the code size does not yield an improvement in the logical error rate when using BP alone. Therefore, post-processing techniques are still necessary to achieve the desired *threshold-like* behavior for the bivariate bicycle codes, as anticipated.

Figure 2 illustrates that the performance of BP+OSD is effectively matched by the BP+BP+OSD approach evaluated here. The key point is that this performance parity is achieved with approximately 90% fewer BP iterations overall. Similarly, the proposed BP+BP+OTF achieves a logical error probability within an order of magnitude of BP+OSD, again using around 90% fewer BP iterations. Furthermore, the OTF post-processor has a proven almost-linear runtime complexity, ensuring that the entire decoding process is extremely fast.

It is also noteworthy that the error curve for BP+BP+OTF steadily diverges from those of BP+OSD and BP+BP+OSD as the code distance increases. This divergence may be due to the larger size of the OTF, which might require additional BP iterations to fully converge. In future work, we plan to investigate the number of BP rounds necessary for BP+BP+OTF to match the performance of running BP+OSD on the detector error model.

VII. CONCLUSION

In this work, we introduced BP+BP+OTF as an almost linear-time decoder for QLDPC codes under circuit-

level noise. The OTF post-processor removes qubits from the decoding graph until it achieves a tree-like structure, thereby increasing the likelihood that subsequent rounds of BP will converge. Additionally, we presented a novel method for mapping detector error models to sparser matrices while preserving critical information about circuit-level fault propagation. Numerical simulations demonstrate that using this mapping, the BP+BP+OTF decoder nearly matches the performance of state-of-the-art decoders such as BP+OSD when applied to families of bivariate bicycle codes under circuit-level noise.

The sparsification routine we propose extends beyond the BP+BP+OTF decoder. Our simulations suggest that performing an initial round of decoding on the full detector model, followed by a second round on the sparsified detector model, can enhance performance across various decoders, including plain BP and BP+OSD. The sparsified detector model features fewer loops, fewer columns, and a less redundant structure. Moreover, by mapping the soft information from the first BP round to the sparsified detector model, the second BP round is supplied with a non-uniform error channel, accelerating convergence. Our results show that this mapping to the sparsified detector model significantly reduces the number of required BP iterations across all the decoders we have investigated. We anticipate that other decoder families – for example BP+AC [16], BP+LSD [18], and BP+CB [17] – will also benefit from the sparsified detector error model.

In future work, we will explore the application of the BP+BP+OTF decoder to various code families, including surface codes, hypergraph product codes [6], and lifted product codes [7]. For surface codes, it would be particularly interesting to investigate whether the sparsified detector error model mapping can enhance the performance of existing decoders, such as those in [27]. For instance, this could involve implementing a BP+BP+Union-Find or BP+BP+MWPM approach.

The primary failure mode of the BP+BP+OTF algo-

rithm arises in cases where the OTF post-processor fails to produce a spanning tree capable of supporting the syndrome, i.e., when $\mathbf{s} \notin \text{IMAGE}(H_{otf})$. The probability of such failures can be reduced by optimising the sparsity of the transfer matrix that maps the detector model to its sparsified form. In this work, we used an exhaustive approach to derive the mapping, but further optimisations could be achieved by, for example, explicitly excluding elements of H_{sdem} that introduce loops. This remains an area for future investigation.

Further improvements in the runtime of BP+BP+OTF could be achieved by exploring parallelisation methods for the tree search step in the OTF post-processor. One possible approach is to combine OTF post-processing with the parallel cluster-growth strategies employed by the BP+LSD decoder [18].

The OTF post-processor operates on the principle that QLDPC decoding can be enhanced by modifying the structure of the decoding graph. Specifically, Kruskal's algorithm is used to identify and eliminate variable nodes that introduce problematic cycles in the Tanner graph. Similarly, the recently introduced BP plus guided decimation (BP+GD) decoder iteratively modifies the decoding graph by excluding variable nodes with the least uncertainty in their soft-information [30]. An interesting direction for future research would be to explore the combination of BP+OTF and BP+GD.

Given its low complexity, BP+BP+OTF is a promising candidate for real-time decoding of syndromes from experimental quantum computers. To this end, dedicated hardware implementations of the algorithm using FPGAs or ASICs will be necessary. Since the BP+BP+OTF algorithm uses standard methods like the well-established product-sum implementation of BP and Kruskal's minimum spanning tree algorithm, it may be possible to construct such a decoder by combining existing commercially available chips. Consequently, development costs could

potentially be lower compared to more specialised decoders such as BP+OSD [31].

VIII. CODE AVAILABILITY

The code for the BP+OTF decoder can be found in the following Github repository: <https://github.com/Ademartio/BPOTF>. In future versions we will include a script for obtaining the transfer matrix, the two-stage BP process and the overall BP+BP+OTF decoder.

IX. ACKNOWLEDGEMENTS

We thank Oscar Higgott for many useful comments and recommendations, as well as Anqi Gong for discussions on loops and trapping sets present in the detector error models of bivariate bicycle codes. We also thank Pedro Crespo for his guidance and the other members of the Quantum Information Group at Tecnum for their support.

This work was supported by the Spanish Ministry of Economy and Competitiveness through the MADDIE project (Grant No. PID2022-137099NBC44), by the Spanish Ministry of Science and Innovation through the project Few-qubit quantum hardware, algorithms and codes, on photonic and solid state systems (PLEC2021-008251), and by the Ministry of Economic Affairs and Digital Transformation of the Spanish Government through the QUANTUM ENIA project call - QUANTUM SPAIN project, and by the European Union through the Recovery, Transformation and Resilience Plan - NextGenerationEU within the framework of the Digital Spain 2026 Agenda. J.R. is funded by the Engineering and Physical Sciences Research Council (Grant codes: EP/T001062/1 and EP/X026167/1).

-
- [1] J. Roffe, "Quantum error correction: an introductory guide," *Contemporary Physics*, vol. 60, no. 3, pp. 226–245, 2019. [Online]. Available: <https://doi.org/10.1080/00107514.2019.1667078>
 - [2] Google Quantum AI, "Quantum error correction below the surface code threshold," 2024. [Online]. Available: <https://arxiv.org/abs/2408.13687>
 - [3] S. Krinner, N. Lacroix, A. Remm, A. Di Paolo, E. Genois, C. Leroux, C. Hellings, S. Lazar, F. Swiadek, J. Herrmann, G. J. Norris, C. K. Andersen, M. Müller, A. Blais, C. Eichler, and A. Wallraff, "Realizing repeated quantum error correction in a distance-three surface code," *Nature*, vol. 605, no. 7911, p. 669–674, May 2022. [Online]. Available: <http://dx.doi.org/10.1038/s41586-022-04566-8>
 - [4] A. deMarti iOlius, P. Fuentes, R. Orús, P. M. Crespo, and J. Etxezarreta Martinez, "Decoding algorithms for surface codes," *arXiv*, Jul. 2023, <https://doi.org/10.48550/arXiv.2307.14989>.
 - [5] S. Bravyi, A. W. Cross, J. M. Gambetta, D. Maslov, P. Rall, and T. J. Yoder, "High-threshold and low-overhead fault-tolerant quantum memory," *Nature*, vol. 627, no. 8005, pp. 778–782, Mar 2024. [Online]. Available: <https://doi.org/10.1038/s41586-024-07107-7>
 - [6] Q. Xu, J. P. B. Ataides, C. A. Pattison, N. Raveendran, D. Bluvstein, J. Wurtz, B. Vasic, M. D. Lukin, L. Jiang, and H. Zhou, "Constant-overhead fault-tolerant quantum computation with reconfigurable atom arrays," 2023. [Online]. Available: <https://arxiv.org/abs/2308.08648>
 - [7] T. R. Scruby, T. Hillmann, and J. Roffe, "High-threshold, low-overhead and single-shot decodable fault-tolerant quantum memory," 2024. [Online]. Available: <https://arxiv.org/abs/2406.14445>
 - [8] T. Richardson and S. Kudekar, "Design of low-density parity check codes for 5g new radio," *IEEE Communications Magazine*, vol. 56, no. 3, pp. 28–34, Mar. 2018. [Online]. Available: <https://ieeexplore.ieee.org/abstract/document/8316763>

- [9] D. J. MacKay and R. M. Neal, “Near Shannon limit performance of low density parity check codes,” *Electronics letters*, vol. 33, no. 6, pp. 457–458, 1997.
- [10] P. Fuentes, J. Etxezarreta Martinez, P. M. Crespo, and J. Garcia-Frías, “Degeneracy and its impact on the decoding of sparse quantum codes,” *IEEE Access*, vol. 9, pp. 89093–89119, 2021. [Online]. Available: <https://ieeexplore.ieee.org/abstract/document/9456887>
- [11] N. Raveendran and B. Vasić, “Trapping Sets of Quantum LDPC Codes,” *Quantum*, vol. 5, p. 562, Oct. 2021. [Online]. Available: <https://doi.org/10.22331/q-2021-10-14-562>
- [12] A. Grospellier, L. Grouès, A. Krishna, and A. Leverrier, “Combining hard and soft decoders for hypergraph product codes,” *Quantum*, vol. 5, p. 432, Apr. 2021. [Online]. Available: <http://dx.doi.org/10.22331/q-2021-04-15-432>
- [13] P. Pantelev and G. Kalachev, “Degenerate quantum ldpc codes with good finite length performance,” *Quantum*, vol. 5, p. 585, Nov. 2021. [Online]. Available: <http://dx.doi.org/10.22331/q-2021-11-22-585>
- [14] J. Roffe, D. R. White, S. Burton, and E. Campbell, “Decoding across the quantum low-density parity-check code landscape,” *Phys. Rev. Res.*, vol. 2, p. 043423, Dec 2020. [Online]. Available: <https://link.aps.org/doi/10.1103/PhysRevResearch.2.043423>
- [15] T. R. Scruby and K. Nemoto, “Local probabilistic decoding of a quantum code,” *Quantum*, vol. 7, p. 1093, Aug. 2023. [Online]. Available: <http://dx.doi.org/10.22331/q-2023-08-29-1093>
- [16] S. Wolanski and B. Barber, “Ambiguity Clustering: an accurate and efficient decoder for qLDPC codes,” *arXiv*, p. arXiv:2406.14527, Jun. 2024, <https://arxiv.org/abs/2406.14527>.
- [17] A. deMarti iOlius and J. Etxezarreta Martinez, “The closed-branch decoder for quantum LDPC codes,” *arXiv*, p. arXiv:2402.01532, Feb. 2024, <https://doi.org/10.48550/arXiv.2402.01532>.
- [18] T. Hillmann, L. Berent, A. O. Quintavalle, J. Eisert, R. Wille, and J. Roffe, “Localized statistics decoding: A parallel decoding algorithm for quantum low-density parity-check codes,” *arXiv*, Jun. 2024, <https://doi.org/10.48550/arXiv.2406.18655>.
- [19] J. B. Kruskal, “On the shortest spanning subtree of a graph and the traveling salesman problem,” *Proceedings of the American Mathematical Society*, vol. 7, no. 1, pp. 48–50, 1956.
- [20] P.-J. H. S. Derks, A. Townsend-Teague, A. G. Burchards, and J. Eisert, “Designing fault-tolerant circuits using detector error models,” *arXiv*, Jul. 2024, <https://doi.org/10.48550/arXiv.2407.13826>.
- [21] Strictly, the number of columns n is not exactly the number of possible circuit errors since errors that have the same detector vectors are merged in single columns, adding their a priori probabilities.
- [22] C. Gidney, “Stim: a fast stabilizer circuit simulator,” *Quantum*, vol. 5, p. 497, Jul. 2021. [Online]. Available: <https://doi.org/10.22331/q-2021-07-06-497>
- [23] W. Fang and M. Ying, “Symbolic execution for quantum error correction programs,” *Proceedings of the ACM on Programming Languages*, vol. 8, no. PLDI, p. 1040–1065, Jun. 2024. [Online]. Available: <http://dx.doi.org/10.1145/3656419>
- [24] M. H. G. Michael T. Goodrich, Roberto Tamassia, *Data Structures and Algorithms in Python*, 1st ed. Wiley, 2013.
- [25] O. Higgott, “Pymatching,” <https://github.com/oscarhiggott/PyMatching>, accessed: 2024-07-26.
- [26] N. Delfosse and N. H. Nickerson, “Almost-linear time decoding algorithm for topological codes,” *Quantum*, vol. 5, p. 595, Dec. 2021. [Online]. Available: <https://doi.org/10.22331/q-2021-12-02-595>
- [27] O. Higgott, T. C. Bohdanowicz, A. Kubica, S. T. Flammia, and E. T. Campbell, “Improved decoding of circuit noise and fragile boundaries of tailored surface codes,” *Phys. Rev. X*, vol. 13, p. 031007, Jul 2023. [Online]. Available: <https://link.aps.org/doi/10.1103/PhysRevX.13.031007>
- [28] Recall that the XOR logical operation is true if and only if the number of true inputs is odd. Furthermore, XOR and modulo-2 sum are equivalent for the binary field, i.e. a parity constraint. We stick to the XOR operation so as to relate the update rule to the Piling-up lemma, which is formulated by means of it [29].
- [29] M. Matsui, “Linear cryptanalysis method for decipher,” in *Advances in Cryptology — EUROCRYPT ’93*, T. Helleseth, Ed. Berlin, Heidelberg: Springer Berlin Heidelberg, 1994, pp. 386–397. [Online]. Available: https://link.springer.com/chapter/10.1007/3-540-48285-7_33
- [30] H. Yao, W. A. Laban, C. Häger, A. G. i Amat, and H. D. Pfister, “Belief propagation decoding of quantum ldpc codes with guided decimation,” 2024. [Online]. Available: <https://arxiv.org/abs/2312.10950>
- [31] J. Valls, F. Garcia-Herrero, N. Raveendran, and B. Vasić, “Syndrome-based min-sum vs osd-0 decoders: Fpga implementation and analysis for quantum ldpc codes,” *IEEE Access*, vol. 9, pp. 138 734–138 743, 2021. [Online]. Available: <https://ieeexplore.ieee.org/document/9562513>
- [32] A. Gong, S. Cammerer, and J. M. Renes, “Toward Low-latency Iterative Decoding of QLDPC Codes Under Circuit-Level Noise,” *arXiv e-prints*, p. arXiv:2403.18901, Mar. 2024, <https://arxiv.org/abs/2403.18901>.
- [33] Being strictly correct, the first round is special due to the fact that there is no propagation of previous rounds and, thus, such first round should be processed independently [32].
- [34] J. Roffe, “LDPC: Python tools for low density parity check codes,” 2022. [Online]. Available: <https://pypi.org/project/ldpc/>

Appendix A: The Union-Find data structure for the OTF decoder

In order to search an OTF in almost-linear time, we need to consider the union find data structure. Let us consider a dynamic list of a length equal to the number of checks in the code to decode, where each element is a 2-element list, we shall name that list as DYNAMIC_LIST. The first element of each tuple will indicate the root of the element and the second one will indicate its depth. At the beginning, each element i will be its own root and its depth will be 1, i.e. $\text{DYNAMIC_LIST}[i] = [i, 1]$. Each element in the dynamic list will become a tree of a

single element. Afterwards, we will consider columns in the parity check matrix in the order established by the posterior probabilities. Once we consider a column in the parity check matrix, we will study its non-trivial elements. Considering j non-trivial elements, we will search at the root of each of them in the `DYNAMIC_LIST`. If the j roots are different, introducing the edges emanating from the variable node which represents the column will not produce a loop in the Tanner graph. If that is the case, all the elements will be merged into a single tree and the root with the largest depth will become the root of the overall tree. Subsequently, the remaining roots will change their first element in the `DYNAMIC_LIST` to be the new root. Moreover, if there are two or more roots with largest depth, one will be chosen arbitrarily to be the new root of the merged tree and its depth will be increased by one.

After the first step, there will be elements in the `DYNAMIC_LIST` for which the first element will not satisfy `DYNAMIC_LIST[i][0] = i`, but the new root that it has adopted once merging with other trees. Therefore, if we want to know its root, we will have to search the first element of the dynamic list of each element that we find until the condition `DYNAMIC_LIST[i][0] = i` is satisfied. Figure 3 portrays an example of the process of considering a column with three non-trivial elements, which results in the merging of three trees.

The objective of the OTF decoder will be to consider all columns from the parity check matrix following this rationale. After all the columns have been considered, the ones that will have been kept for the OTF matrix will not produce loops in the Tanner graph. Ultimately, this process will involve considering n columns from the parity check matrix, for each column to consider j non-trivial elements, and for each of these elements to look for their root, which can be done in, at most, $\log(n)$ time. Therefore, the overall worst-case complexity of the process of searching an OTF given a parity check matrix is $\mathcal{O}(nj \log(n))$. Due to the fact that the weight of the column is assumed to be constant when increasing block length, the overall complexity can be expressed as $\mathcal{O}(n \log(n))$.

Appendix B: Finding the transfer matrix by means of an exhaustive search

We aim the decomposition of each column of the detector error model into a minimum amount of sparsified components by means of the exhaustive search shown in Algorithm 3. The algorithm starts by identifying the columns of H_{sdem} that at least share a non-trivial component with the selected detector error model column, saved in the $H_{reduced}$ matrix. This is done to reduce the amount of elements to be considered in the exhaustive search. Once this is done, the algorithm starts to test if the detector vector in question can be expressed as a combination of the columns of the sparsified parity check

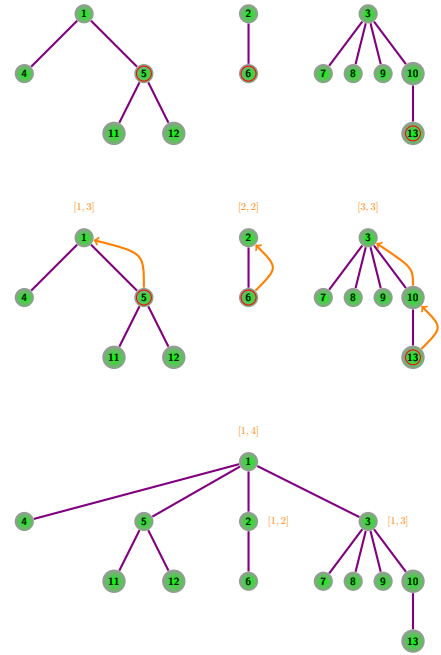


Figure 3: Process of considering a column in the parity check matrix for the ordered Tanner forest. Green circles represent the elements of the `DYNAMIC_LIST`, which are labelled. For a violet line connecting a node on the bottom j with a bottom on the top i , `DYNAMIC_LIST[j][0] = i`. The **top** figure indicates three trees with three different roots on the top. The three red-circled nodes belong to the non-trivial elements of the column that is being considered. On the **middle** image, the value of the three roots of each considered node is found within the `DYNAMIC_LIST`. Since all roots are different, we can incorporate the column, as it does not produce a loop. We choose the root of the tree on the left as the overall root and, in the **bottom** figure, we merge the three trees by changing the first element in the `DYNAMIC_LIST` of the elements 2 and 3 to be 1. Moreover, as the tree on the left and the one on the right had the same depth, the depth of the overall tree increases by 1 to be 4.

matrix, starting from a single element in the sum and progressively increasing the amount of terms in the decomposition. This is done in the for loop of starting at line 17. The `GetCombinations([1, 2, ..., cols_r], j)` method creates a matrix containing all possible combinations with size j of the elements of the vector $[1, 2, \dots, cols_r]$ as its rows. When we write `combs(k)`, we refer to getting a row of such matrix, i.e. a possible combination of columns with indexes given by such row. Therefore, the matrix obtained has size $\binom{cols_r}{j} \times j$, and we use those combinations to test the decomposition with j elements and increase such value if no decomposition is found. We also impose that a decomposition candidate must co-

Algorithm3 Decomposing detector error model detectors into “phenomenological” elements

INPUT: detector error model column $\mathbf{h}_{dem}^i \in \mathbb{F}_2^d$,
 “phenomenological” parity check matrix
 $H_{sdem} = (\mathbf{h}_{sdem}^1, \dots, \mathbf{h}_{sdem}^{n_s}) \in \mathbb{F}_2^{d \times n_s}$,
 logical observable detector error model matrix $O_{dem} \in \mathbb{F}_2^{k \times n}$,
 logical observable “phenomenological” matrix
 $O_{sdem} \in \mathbb{F}_2^{k \times n_s}$
OUTPUT: decomposition vector for the detector error
 model column, $\mathbf{a}^i \in \mathbb{F}_2^{n_s}$

```

1:                                     ▷ Get columns of  $H_{sdem}$  that at least
   share a non-trivial element with the detector error model
   column,  $\mathbf{h}_{dem}^i$ . The map variable contains which elements
   of  $H_{sdem}$  are retained so that the result for  $H_{reduced}$  can
   be mapped back.
2:  $H_{reduced} \leftarrow \emptyset$ 
3:  $O_{reduced} \leftarrow \emptyset$ 
4:  $map \leftarrow \emptyset$ 
5: for  $j \leftarrow 1$  to  $n_s$  do
6:   for  $k \leftarrow 1$  to  $d$  do
7:     if  $\mathbf{h}_{dem}^i(k) == \mathbf{h}_{sdem}^j(k)$  &  $\mathbf{h}_{dem}^i(k) == 1$  then
8:        $H_{reduced} \leftarrow H_{reduced} \cup \mathbf{h}_{sdem}^j$ 
9:        $O_{reduced} \leftarrow O_{reduced} \cup \mathbf{o}_{sdem}^j$ 
10:       $map \leftarrow map \cup \{j\}$ 
11:     break
12:   end if
13: end for
14: end for
15:                                     ▷ Exhaustive search over
   the reduced matrix  $H_{reduced}$  to decompose the detector
   error model column,  $\mathbf{h}_{dem}^i$ .  $cols_r$  refers to the number of
   columns of  $H_{reduced} = (\mathbf{h}_{reduced}^1, \dots, \mathbf{h}_{reduced}^{cols_r})$ . Vectors
    $\mathbf{e}_{dem}^i, \mathbf{e}_{reduced}^m$  refer to the error vectors associated to the
    $i$  and  $m$  columns of their respective parity check matrix.
16:  $\mathbf{a}^i \leftarrow \emptyset$ 
17: for  $j \leftarrow 1$  to  $cols_r$  do
18:    $combs \leftarrow \text{GetCombinations}([1, 2, \dots, cols_r], j)$ 
19:   for  $k \leftarrow 1$  to  $\binom{cols_r}{j}$  do
20:      $dec \leftarrow \sum_{m \in combs(k)} \mathbf{h}_{reduced}^m$ 
21:      $\mathbf{e}_{dec} \leftarrow \sum_{m \in combs(k)} \mathbf{e}_{reduced}^m$ 
22:      $\mathbf{l}_{sdem} \leftarrow O_{reduced} \cdot \mathbf{e}_{dec}$ 
23:      $\mathbf{l}_{dem} \leftarrow O_{dem} \cdot \mathbf{e}_{dem}^i$ 
24:     if ( $dec == \mathbf{h}_{dem}^i$  &  $\mathbf{l}_{sdem} == \mathbf{l}_{dem}$ ) then
25:        $\mathbf{a}^i = ones(map(combs(k)))$ 
26:     break
27:   end if
28:   if  $\mathbf{a}^i \neq \emptyset$  then
29:     break
30:   end if
31: end for
32: end for
33: return  $\mathbf{a}^i$ 

```

incide in its logical effect. Once such a decomposition is found, we generate the decomposition vector \mathbf{a}^i with the method $ones(map(combs(k)))$ which adds ones at locations $map(combs(k))$, i.e. at the positions found but mapped back from the $H_{reduced}$ to the H_{sdem} of inter-

est. Note that since we exhaustively search from a minimum amount of columns to a bigger one, the obtained decomposition is expected to be consisted of a minimum amount of sparsified mechanisms.

Algorithm 3 is then looped for all the columns of the detector error model in question and a transfer matrix A_{tr} is found, relating the detector error model and the sparsified parity check matrix of interest. The exhaustive search approach seems to be demanding due to the fact that the combinatorial number $\binom{cols_r}{j}$ increases very fast with j . However, for all the codes considered in this article, the number of elements in the decomposition has not exceeded 3 components and, thus, it is relatively fast. Importantly, this is done in a pre-processing stage and has not impact in the latency of the decoder. Note, also, that detector error model matrices have a periodic structure from round to round, as it can be seen in Figure 1 of [32], implying that the processing can be done for a single propagation round and then extrapolate the rest of the transfer matrix [33]. It is not within the scope of this work to optimize this decomposition, but to show that doing this kind of reduction to a sparsified noise model is beneficial to decode over circuit-level noise. Aiming at the best decomposition and finding better ways to search for those, e.g. using stabiliser simulators such as Stim, is considered future work.

Appendix C: Numerical simulations

Monte Carlo computer simulations of the bivariate bicycle codes have been performed with the objective of obtaining the performance curves (logical error rate). The circuit-level noise simulations have been done the following way. The sampling of the errors arising due to the noisy stabiliser circuit noise has been done by means of Stim [22]. Stim considers the check measurements upon a set of syndrome extractions altogether with a final measurement of the data qubits. We consider d_c syndrome extraction rounds, where d_c is the distance of the QEC. We also use the SlidingWindowDecoding [32] Github repository for constructing the Stim syndrome extraction circuits and obtain the circuit-level noise parity check and observable matrices of the bivariate bicycle codes. The decoder uses those to resolve the syndrome and return an error, which is later compared to the logical action of the Stim error.

The operational figure of merit we use to evaluate the performance of these quantum error correction schemes is the Logical Error Rate per syndrome cycle (P_L), i.e. the probability that a logical error has occurred after the recovery operation per syndrome extraction round [5].

Regarding the software implementations of the decoders used perform the numerical simulations have been: the BP+OSD implementation in the LDPC Github package [14, 34] (with slight modifications for handling circuit-level noise [5]) and our implementation for the proposed decoder can be found in the following Github

<https://github.com/Ademartio/BPOTF>.

For the numerical Monte Carlo methods employed to estimate the logical error probability per syndrome cycle, P_L , we have applied the following rule of thumb to select the number of simulation runs, N_{runs} [4], to get the logical error rate for d_c syndrome extraction rounds, $P_L(d_c)$, as

$$N_{\text{runs}} = \frac{100}{P_L(d_c)}. \quad (\text{C1})$$

As explained in [4], under the assumption that the observed error events are independent, this results in a 95% confidence interval of about $(0.8\hat{P}_L(d_c), 1.25\hat{P}_L(d_c))$, where $\hat{P}_L(d_c)$ refers to the empirically estimated value for the logical error rate. The final P_L is just obtained by dividing the numerically estimated value by the number of syndrome extraction cycles, i.e. $P_L = \hat{P}_L(d_c)/d_c$. [5].

Appendix D: Circuit-level noise model

We consider the standard depolarizing (unbiased) circuit-level noise model [4, 5, 27, 32] that consists of:

- **Decoherence errors:** data qubits are subjected to depolarizing noise before syndrome ex-

traction round, i.e. $\{I, X, Y, Z\}$, sampled independently with probabilities $p_X = p_Y = p_Z = p/3$ and $p_I = 1 - p$.

- **Noisy single qubit gates:** those are followed by a Pauli operator, $\{I, X, Y, Z\}$, sampled independently with probabilities $p_X = p_Y = p_Z = p/3$ and $p_I = 1 - p$.
- **Noisy two-qubit gates:** those are followed by a two-qubit Pauli operator, $\{I, X, Y, Z\}^{\otimes 2}$, sampled independently with probability $p/15$ for the non-trivial operators and $p_{I^{\otimes 2}} = 1 - p$.
- **State preparation:** state preparations are followed by a Pauli operator which may flipped the state to its orthogonal one with probability p . Note that this reduces to substituting the preparation of the $|0\rangle$ state by $|1\rangle$ and the preparation of the $|+\rangle$ state by $|-\rangle$, each with probability p .
- **Measurements:** the outcomes of measurements are flipped with probability p .
- **Idle gate (memory) locations:** those are followed by a Pauli operator, $\{I, X, Y, Z\}$, sampled independently with probabilities $p_X = p_Y = p_Z = p/3$ and $p_I = 1 - p$.